Chemical Science

EDGE ARTICLE

View Article Online
View Journal | View Issue

Cite this: *Chem. Sci.*, 2016, **7**, 4698

Tetrathiafulvalene-containing polymers for simultaneous non-covalent modification and electronic modulation of MoS_2 nanomaterials†

Ryan C. Selhorst,‡[a] Egle Puodziukynaite,‡[a] Jeffrey A. Dewey,[a] Peijian Wang,[b] Michael D. Barnes,[b] Ashwin Ramasubramaniam[c] and Todd Emrick*[a]

Received 21st January 2016
Accepted 5th April 2016

DOI: 10.1039/c6sc00305b

www.rsc.org/chemicalscience

Transition metal dichalcogenides (TMDCs) such as MoS_2 comprise an important class of 2D semiconductors with numerous interesting electronic and mechanical features. Full utilization of TMDCs in materials and devices, however, necessitates robust functionalization methods. We report well-defined tetrathiafulvalene (TTF)-based polymers, exploiting synthetic routes that overcome challenges previously associated with these systems. These platforms enable basal plane coordinative interactions with MoS_2, conceptually in parallel with pyrene-containing platforms for graphene and carbon nanotube modification. Not yet reported for TMDCs, these non-covalent interactions are universal and effective for MoS_2 irrespective of the lattice structure, affording significantly enhanced solution stabilization of the nanosheets. Additionally, the TTF-functionalized polymers offer electronic structure modulation of MoS_2 by ground state charge transfer and work function reduction, demonstrated using Kelvin probe force microscopy (KPFM). Notably, coordination and electronic effects are amplified for the TTF–polymers over TTF itself. Experiments are supported by first-principles density functional theory (DFT) calculations that probe polymer–TTF surface interactions with MoS_2 and the resultant impact on electronic properties.

Introduction

Electronically active 2-D materials have emerged as promising architectural elements of next generation optoelectronic devices, combining desirable electronic and quantum effects with robust mechanical properties.[1–4] For example, extensive research is now directed towards graphene to aid its integration into devices and exploit its unique optoelectronic properties. However, an inherent drawback to graphene is the absence of a bandgap, which limits its applicability in digital logic.[5–7] Molybdenum disulfide (MoS_2), a transition metal dichalcogenide (TMDC), represents an example of an alternative class of 2-D materials behaving as semiconductors and thus offers an energy gap from 1.2 eV (bulk) to 1.9 eV (atomically thin), and an intrinsic photoluminescence not found in graphene.[6,8] MoS_2 thus holds promise in next-generation field effect transistors, biosensors, light-emitting diodes, and energy storage devices.

A future integration of MoS_2 nanomaterials into electronic materials hinges on modulating their processibility and electronic properties through surface functionalization. The ability to process MoS_2 nanosheets from a variety of solvents would advance applications in sensing, electroactive inks, thermoelectrics and solution-processible electronics.[9,10] Numerous examples of covalent and non-covalent modification of graphene are known,[11–15] but reports on TMDC functionalization are relatively scarce. For example, Huang and Dravid described the modification of chemically exfoliated MoS_2 nanosheets with PEG-thiol to afford aqueous suspensions;[16] however, these thiol–surface interactions require Mo-rich TMDC edges and surface defects (S vacancies). Moreover, electrostatic interactions of MoS_2 and cationic surfactants have been exploited to enhance thermal and mechanical stability of polymer nanocomposites, but still require surface defects to facilitate functionalization.[17] Alternatively, non-covalent approaches to MoS_2 (basal plane) functionalization are lacking, though the development of such methods would preserve the pristine lattice of the nanostructures, conceptually in parallel to pyrene modification of graphene and carbon nanotubes.[18] Surface adsorbates can additionally modify the band structure of TMDCs,[19] which is desirable since MoS_2 possesses lower charge mobility than graphene, with applications in sensing, catalysis and spintronics/valleytronics requiring dopants (*i.e.*, inorganic ions, tertiary amines, ionic liquids and small molecule electron donors).[20–23] In one example, Javey and coworkers used benzyl

[a]*Polymer Science and Engineering Department, 120 Governors Drive, Amherst, Massachusetts 01003, USA. E-mail: tsemrick@mail.pse.umass.edu*

[b]*Department of Chemistry, University of Massachusetts, 710 North Pleasant Street, Amherst, MA 01003, USA*

[c]*Department of Mechanical and Industrial Engineering University of Massachusetts, Amherst, 160 Governors Drive Amherst, MA 01003, USA*

† Electronic supplementary information (ESI) available. See DOI: 10.1039/c6sc00305b

‡ These authors contributed equally to the manuscript.

viologen, a small molecule donor, to n-dope MoS_2. The extent of doping was probed through fabrication of FETs to demonstrate the efficacy of such non-covalent functionalization.[24] Despite recent progress, the need remains for simple routes to novel TMDC dopants that simultaneously afford solution processible and electronically robust TMDC-based hybrid architectures.

Here we describe the preparation of tetrathiafulvalene (TTF)-substituted polymers to solubilize MoS_2 nanosheets as envisaged in Fig. 1. TTF is a sulfur-rich electron donor with oxidation potentials at 0.37 and 0.70 V (*vs.* Ag/AgCl SRE), offering n-doping when in contact with 2-D materials.[25,26] The sulfur- and electron-rich structure of TTF is attractive for inducing non-covalent interactions with MoS_2, including S–S, S–Mo, and S–π coordination, as well as binding through charge transfer. While we anticipated that polymers featuring pendent TTF moieties may function in multi-point basal plane coordinative interactions with MoS_2, we and others find the preparation of such polymers challenging synthetically due to limitations imposed by TTF itself on free radical and ionic polymerization techniques, generally low yielding processes affording ill-characterized products.[27–29]

Our synthetic approach to TTF-containing polymers circumvents prior limitations, yielding a novel polymer platform with tunable TTF incorporation and benefitting from the solution processibility offered by an aliphatic polymer backbone. We report two examples, one in which a TTF-substituted polynorbornene was prepared by ring opening metathesis polymerization (ROMP), and a second consisting of TTF-substituted methacrylate polymers prepared by reversible addition–fragmentation chain-transfer (RAFT) polymerization and post-polymerization cycloaddition. These polymers possess tunable electronic properties dictated by TTF density and comonomer selection, imparting solution stability and band structure modulation to MoS_2 nanomaterials. The experiments described were performed in conjunction with density functional theory (DFT) calculations that probe MoS_2 surface interactions and their impact on electronic properties.

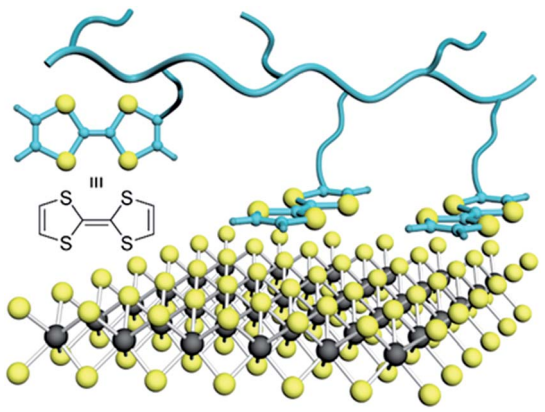

Fig. 1 Physisorption of TTF on MoS_2: schematic illustration of TTF-containing polymers interacting with MoS_2 nanosheets. The dark and yellow spheres represent Mo and S atoms, respectively.

Results and discussion

TTF-norbornene **2**, shown in Scheme 1, was prepared by carbodiimide coupling of 2-hydroxymethyl TTF **1** with *exo*-5-norbornene carboxylic acid. While attempted ROMP of monomer **2** using the 3-bromopyridine-substituted ruthenium benzylidene catalyst[30] produced insoluble material, copolymerization of **2** with *n*-hexyl-substituted norbornene **3** gave soluble polymers, albeit with a broad, multi-modal molecular weight distribution evident from gel permeation chromatography (GPC) characterization. In each case, sulfur-metal interactions may complicate clean, productive metathesis, a feature noted for other sulfur-containing cyclic olefins.[31] Fortunately, polymerizations proceeded smoothly when using Grubbs 'Generation I' catalyst and PPh_3 as an auxiliary ligand (the added ligand intended to increase the rate of initiation relative to propagation, or k_i/k_p).[32] Copolymerization of **2** with *n*-hexyl ester **3** proceeded smoothly, affording poly(TTF–norbornene)s **4a–e** with estimated molecular weights in the 20–60 kDa range and PDI values of 1.1–1.3. The successful incorporation of TTF into the polymers was confirmed by ^{1}H NMR spectroscopy, with TTF olefin signals at 6.29–6.30 ppm, and the CH_2 linker resonance at 4.79 ppm. A *cis*/*trans* ratio of 1 : 5 was identified for the unsaturated polyolefins from resonances at 5.20 (*cis*) and 5.35 (*trans*) ppm.

The second synthetic approach, outlined in Scheme 2, produced poly(TTF–methacrylate)s (**9a–h**) by post-polymerization cycloaddition of poly(azidoethyl methacrylate)s **8a–h** with alkyne-substituted TTF **6a**, the latter prepared by reaction of **1** with propargyl bromide. The polymer precursors were synthesized by RAFT polymerization of 2-chloroethyl methacrylate with methyl methacrylate (MMA) or *n*-butyl methacrylate (BMA) comonomers, and the pendent chlorides subsequently displaced by azides. Cycloaddition of TTF-alkyne **6** and the azide-substituted polymers gave poly(TTF–methacrylate)s (M_n 20–40 kDa; PDI 1.1–1.3) in high yield, with excellent azide-to-triazole conversion indicated by ^{1}H NMR spectroscopy (*i.e.*, loss of $C\underline{H}_2N_3$ resonance at 3.51 ppm and appearance of triazole proton

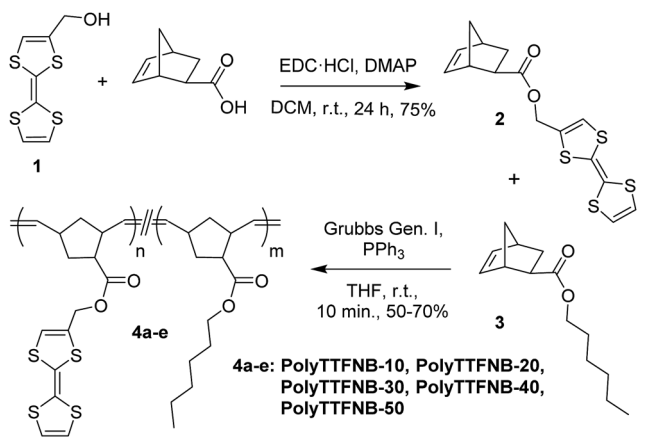

Scheme 1 Synthesis of poly(TTF–norbornene)s by ROMP: (EDC = 1-ethyl-3-(3-dimethylaminopropyl)carbodiimide; DMAP = *N*,*N*-dimethyl-4-aminopyridine). The number of each compound denotes the mole percent incorporation of the TTF-containing repeat units.

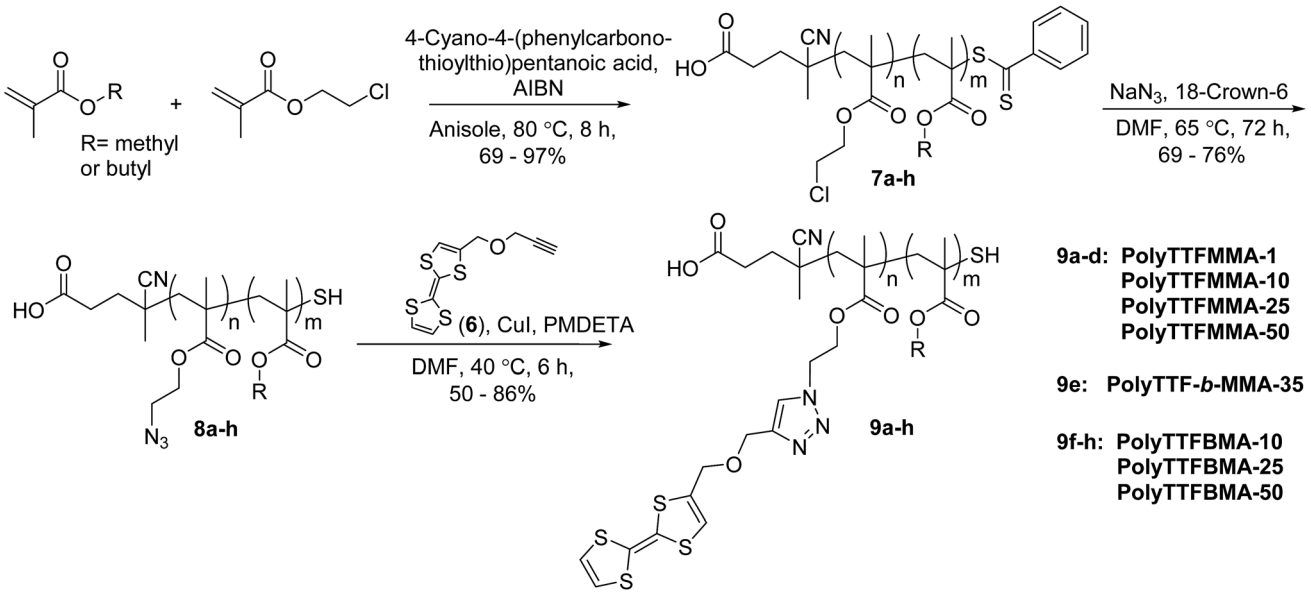

Scheme 2 Preparation of TTF methacrylate polymers (**9a–h**): synthesis of TTF-containing copolymers by RAFT, followed by post-polymerization cycloaddition. The numbers in the compound titles for **9a–h** denote the mole percent incorporation of the TTF-containing repeat units.

at 7.75 ppm). Efficient TTF incorporation was additionally confirmed by the presence of TTF olefin resonances at 6.31 and 6.33 ppm, and the methylene groups of the linker at 4.33 and 4.69 ppm. Notably, this approach allows access to block copolymers, which we prepared containing ~35 mole percent of pendent TTF groups. For electrochemical characterization (described later), a methoxymethyl-substituted derivative of TTF **10** was also prepared (Fig. S4†).

(Spectro)electrochemistry

Electrochemical features of these TTF-containing polymers were examined using cyclic voltammetry in 0.1 M Bu_4NPF_6 solution in *N*-methylpyrrolidone (NMP), using a Pt button, Pt wire, and non-aqueous Ag/Ag^+ electrode (calibrated *vs.* the ferrocene/ferrocenium redox couple) as working, counter, and reference electrodes, respectively. In accord with literature reports, two reversible one-electron oxidation transitions at 0.21 and 0.53 V were observed for TTF itself (Fig. 2a), attributed to its low lying HOMO and subsequent aromatization following electron removal. Model compound **10** exhibited similar electrochemistry, with oxidation at 0.24 and 0.55 V. Notably, the TTF-substituted polymers displayed different redox properties that hinged on TTF density and backbone selection (Fig. 2b). For example, irrespective of percent TTF incorporation, the poly(TTF norbornene)s **4a–e** exhibited one reversible oxidation band at $E_{1/2}$ = 0.25 V. Oxidation to the TTF dication would require high local concentrations of the doubly charged species along the polymer backbone. The TTF radical cation is also known to interact with a neutral TTF to afford mixed valence dimers, which then oxidize to dimer dications (π-dimers).[33,34] These π-dimers exist over a wide electrochemical window with initial oxidation occurring at potentials similar to those required for the TTF/TTF^+ redox couple. We speculate that the absence of a second oxidation peak for the TTF–NB series is also due to the formation of these dimers. For the TTF-containing methacrylates and butyl methacrylates **9a–h**, a second oxidation wave was evident, though attenuated in current density. However, the decrease in peak definition at lower scan rates and quasi reversibility of this transition indicates a possible competition between the formation of TTF^{2+} and aggregated species. Generally, the TTF-based methacrylate polymers had slightly lower oxidation potentials ($E_{1/2}$ = 0.21 V) than the norbornenes, possibly due to a greater steric accessibility of the redox active sites.

The electrochemically-induced redox species were examined further by *in situ* spectroelectrochemistry in 0.1 M Bu_4NPF_6/acetonitrile solutions. Polymer **4e** was dropcast on a transparent indium tin oxide (ITO)/glass working electrode, and silver and platinum wires were used as the reference and counter electrodes, respectively. As evident in Fig. 2c, optical signatures of multiple redox species arose: radical cation (440 and 580 nm), dimer dication (405, 520, 780 nm) and dication (380 nm). Notably, minimal temporal separation was observed between the formation of these species, and no evidence for the sole existence of TTF^{2+} was found even at high electrochemical potentials. Such findings suggest a concerted redox transition and significant destabilization of the second electron oxidation event. While the redox behavior of TTF is complex and dependent on its local environment, all of the TTF-containing polymer systems evaluated oxidize at low electrochemical potential, and thus are suitable for n-doping of TMDC nanosheets.

TTF–MoS_2 interactions: theoretical considerations

Density functional theory (DFT) calculations lend further insight into TTF interactions with MoS_2 and the accompanying

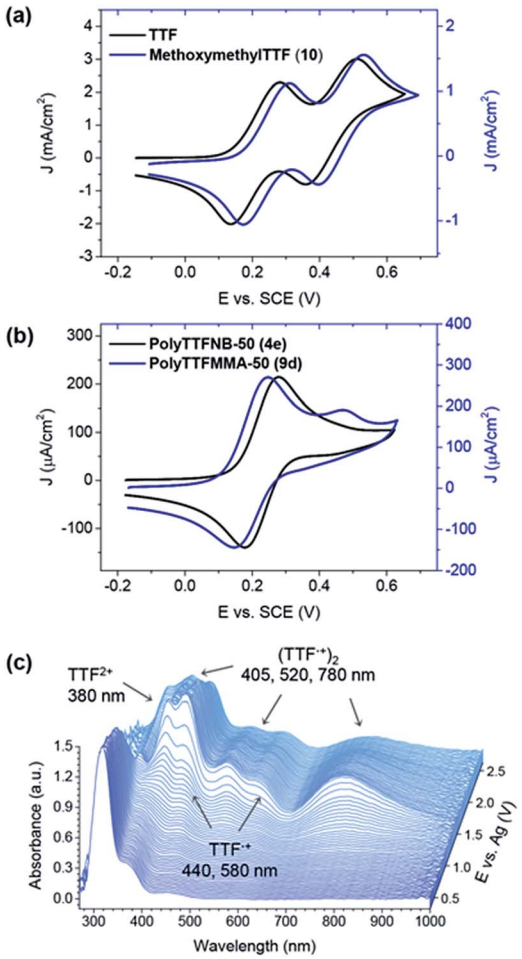

Fig. 2 Electrochemistry of TTF-containing polymers. Cyclic voltammograms of: (a) TTF and methoxymethyl TTF **10** at a 200 mV s^{-1} scan rate, (b) poly(TTF norbornene) **4e** and poly(TTF methacrylate) **9d** at a 200 mV s^{-1} scan rate recorded in a 0.1 M Bu_4NPF_6 NMP solution using a Pt button, non-aqueous Ag/Ag^+ (calibrated *vs.* standard Fc/Fc^+ redox couple) and Pt wire as working, reference and counter electrodes, respectively; and (c) *in situ* spectroelectrochemistry data for a film of **4e** immersed in a 0.1 M Bu_4NPF_6/CH_3CN solution using ITO/glass, Ag and Pt wires as working, reference and counter electrodes, respectively.

electronic effects (computational details given in the ESI†). Scenarios considered for TTF adsorption onto MoS_2 (Fig. 3) include (i) adsorption of a TTF molecule on monolayer MoS_2, (ii) adsorption of a TTF dimer on monolayer MoS_2, and (iii) adsorption of a single TTF molecule at a sulfur vacancy on the basal plane of monolayer MoS_2. These scenarios mimic the experimentally encountered TTF interactions with 2H semiconducting MoS_2 lattices, as well as the effect of these chromophores being in close proximity on a polymeric scaffold. Table S4† displays the adsorption energies, charge transfer, and work function shifts for each of these cases. The large (negative) adsorption energy (~1 eV) indicates strong TTF interactions with the MoS_2 basal plane, even in the absence of surface defects. The small difference (~70 meV) in TTF adsorption on the 4×4 and 8×8 MoS_2 surfaces (4×4 and 8×8 denoting the number of Mo atoms in the surface lattice) suggests a sufficiently dilute coverage so as to neglect inter-adsorbate interactions. The introduction of a basal-plane sulfur vacancy increases TTF binding by ~0.2 eV, and reveals a potential mechanism for suspension stabilization of chemically-exfoliated MoS_2 sheets (which are prone to point defects). The TTF dimer also binds strongly (~1 eV) in the absence of basal plane defects, with calculations supporting TTF–MoS_2 thermodynamics to be sufficiently robust for surface wetting.

The ability of TTF to stabilize MoS_2 suspensions couples with a profound effect of these pendent groups on the electronic properties of MoS_2 nanosheets. For all adsorption scenarios considered, TTF donates electrons (~10^{13} cm^{-2}; Table S4†) to the MoS_2 monolayer (n-doping), seen in the charge-density difference plots of Fig. 3a, c and e, with yellow and cyan indicating charge accumulation and depletion, respectively. The extent of charge transfer is enhanced appreciably by the presence of basal-plane sulfur vacancy defects (*i.e.* larger charge accumulation regions for defective MoS_2) that presumably act as TTF absorption sites. An examination of the density of states of the TTF–MoS_2 composites (red traces in Fig. 3b, d and f) reveals the introduction of flat, dispersionless TTF levels close to the conduction band edge of the pristine MoS_2 monolayer (Fig. 3b); the Fermi level lying near the MoS_2 conduction band edge is consistent with n-doping. However, for an MoS_2 monolayer with a sulfur vacancy (Fig. 3d), the TTF level merges with the vacancy defect level within the band gap of MoS_2, the Fermi level now being pinned at this energy. While the extent of charge transfer is greater in this case, the vacancy defect may function as a deep trap affecting charge conduction through MoS_2. As expected for n-doping, we find a considerable decrease in the work-function of MoS_2 ranging from 1.2 eV for the defective monolayer to 1.8 eV for TTF dimer adsorption. The magnitude of these shifts reflects an idealized situation of a freestanding MoS_2 monolayer and should be interpreted as an upper bound – variations in MoS_2 layer thickness, adsorbate coverage, and substrate-doping effects will impact experimental findings. Nevertheless, qualitative trends observed in work function and charge transfer are consistent with experiments, and the sensitivity of calculations to the selection of DFT exchange–correlation functionals is discussed further in the ESI† (qualitative trends consistent with those presented).

Dispersion of MoS_2 nanosheets with TTF-substituted polymers

The ability of TTF-substituted polymers to disperse MoS_2 was probed using chemically exfoliated MoS_2 nanosheets, prepared using *n*-BuLi as the intercalating agent.[35] Atomic force microscopy (AFM) characterization indicated an average thickness of 0.8–1.5 nm, consistent with 1–2 MoS_2 layers (Fig. S10†).[36,37] The presence of a disordered 1T lattice in the chemically exfoliated MoS_2 nanosheets was confirmed by high resolution transmission electron microscopy (HRTEM, Fig. S11†). The resulting MoS_2 nanosheets were isolated by centrifuging 1 mL of the 1 mg mL^{-1} aqueous suspension (11 200 rcf, 30 min) followed by redispersion in 1.5 mL of the TTF-containing polymer solutions

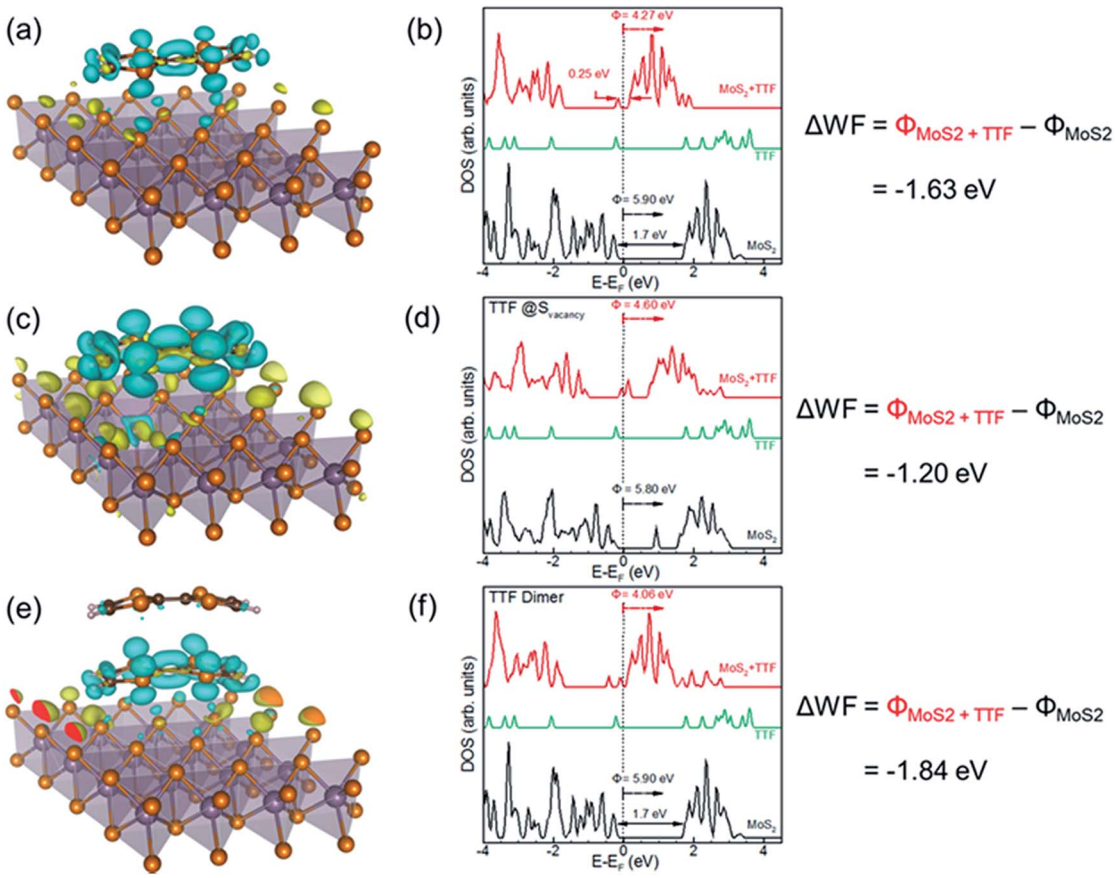

Fig. 3 DFT computations for TTF adsorption on MoS_2. Charge-density difference and density of states plots for a single TTF molecule (a, b) adsorbed on monolayer MoS_2, a single TTF molecule adsorbed at a basal-plane sulfur vacancy defect (c, d) in monolayer MoS_2, and a TTF dimer adsorbed on monolayer MoS_2 (e, f). (a, c, e) Yellow/cyan isosurfaces plotted at $\pm 2.7 \times 10^{-3}$ e Å^{-3} indicate charge accumulation/depletion. (b, d, f) Work functions values (Φ) for the MoS_2 monolayer and the MoS_2/TTF composite are indicated from which we note a decrease in work function of MoS_2 in the presence of the TTF-containing polymers.

(1 mg mL^{-1} in THF) aided by low power sonication; control experiments employed 1 mg mL^{-1} THF solutions of PMMA, PBMA, and poly(*n*-hexyl norbornene) (**5**). Fig. 4 confirms the presence of TTF moieties in the polymers to be crucial for suspension stability. The MoS_2 nanosheets in the control experiments exhibited poor stability, with irreversible precipitation (restacking) observed within hours. In sharp contrast, TTF polymer–MoS_2 suspensions maintained colloidal stability over several weeks, with greater mole percent TTF inclusion affording greater stability. Optical microscopy confirmed such stability, showing dispersed MoS_2 nanostructures from the TTF–polymer solutions (Fig. 4f), and large (hundreds of microns) aggregates for the control systems (Fig. 4e). The poly(TTF methacrylate) series proved optimal, as even a low TTF incorporation of 1 mole percent maintained nanosheet suspensions for several days. Interestingly, block copolymer **9e** did not stabilize the nanosheets for as long a time period as the random polymers, possibly due to a competition between inter-TTF and TTF-MoS_2 interactions. We note that a pyrene-containing methacrylate copolymer containing 12 mole percent pyrene-substituted methacrylate did not enable nanosheet suspension in solution, suggesting that S–S and S–Mo interactions are more influential than S–π interactions for stabilizing chemically exfoliated MoS_2 nanosheets.

The polymer–TTF/MoS_2 nanocomposites were probed by FT-IR spectroscopy to confirm the presence of polymer on the MoS_2 nanosheets. The polymer–TTF/MoS_2 suspensions were subjected to three centrifugation and redispersion cycles to remove excess polymer, and the resultant nanocomposites used for analysis (Fig. S17†). Signals due to polymer adsorption at 2800–3000 cm^{-1} (alkyl C–H stretch), and 1723 cm^{-1} (carbonyl C=O stretch) were retained for these hybrid systems, suggesting that TTF–MoS_2 interactions are maintained during centrifugation/redispersion. Thus, these TTF moieties provide a non-covalently interacting system that can be viewed as analogous to graphene–pyrene coordination and may open new opportunities to realize solution processible MoS_2 nanocomposites.

TTF–MoS_2 electronic interactions

The UV-vis absorption signatures of the chemically exfoliated MoS_2 suspensions (spectra for **polyTTFMMA-25** given in ESI†) resembled the superimposition of the two components, indicating an absence of ground state electronic interactions. This

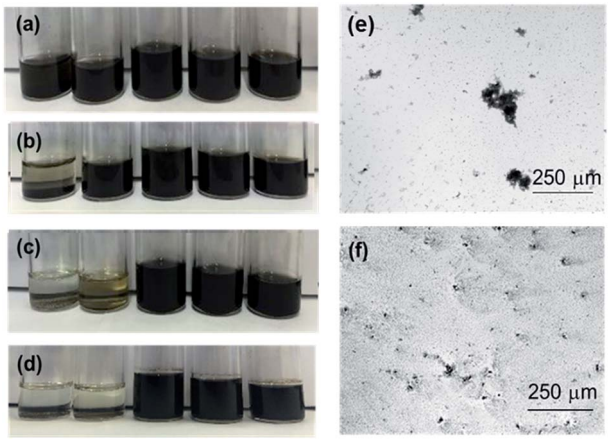

Fig. 4 Solution stabilization of chemically exfoliated MoS_2 nanosheets. Photographs of chemically exfoliated MoS_2/**polyTTFMMA** (**9a–d**) suspensions in THF, taken (a) immediately after preparation, then after (b) 3 days, (c) 5 days, and (d) 18 days. From left to right the polymers used for suspension stabilization are: **PMMA**, **polyTTFMMA-1** (**9a**), **polyTTFMMA-10** (**9b**), **polyTTFMMA-25** (**9c**), **polyTTFMMA-50** (**9d**). Optical micrographs of (e) MoS_2/**PMMA** control in THF and (f) MoS_2/**polyTTFMMA-25** (**9c**) dropcast on glass slides from a THF suspension.

is likely due to lattice disruption in chemically exfoliated semimetallic MoS_2. Thus, we employed a mild MoS_2 exfoliation by sonicating MoS_2 powder in NMP. MoS_2 nanosheets with 2H symmetry and a sulfur-rich basal plane characteristic of the semiconducting allotrope were confirmed by high resolution TEM (Fig. S11a†). The resulting suspensions were subjected to *in situ* UV-VIS experiments upon addition of TTF in NMP. As shown in Fig. 5a, TTF radical cation absorption peaks evolved at 440 and 580 nm, indicating ground state electron transfer from TTF to MoS_2. At later times, the relative intensities of the peaks

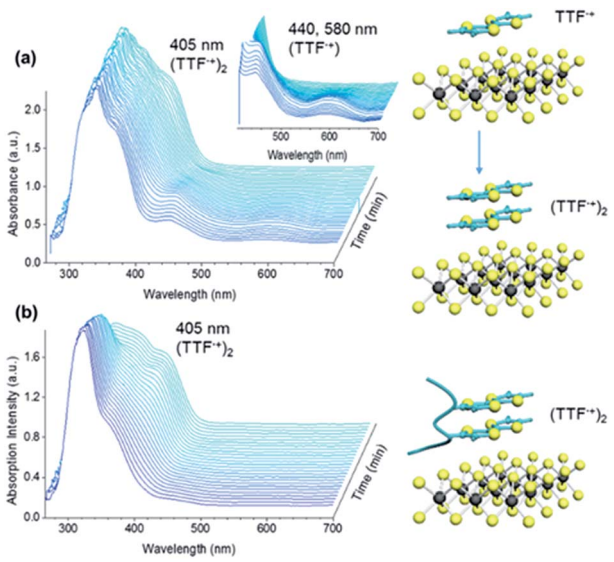

Fig. 5 Spectral evolution of TTF and TTF–polymers on MoS_2. Temporal evolution of UV-VIS absorption spectra of MoS_2 suspensions in NMP upon addition of (a) TTF and (b) **polyTTFMMA-50** (**4e**).

decreased, and a strong signal evolved at 405 nm, characteristic of an intramolecular transition of the TTF pi-dimer.[38,39] Similar to the electrochemistry results, this may be facilitated by $TTF^{+\bullet}$–TTF dimerization possibly followed by a second electron transfer event occurring at identical electrochemical potential. Treating MoS_2 suspensions with the TTF–polymers (example of **polyTTFMMA-50** (**9d**) is given in Fig. 5b) resulted in no radical cation features, and instead a replacement of the neutral TTF absorption at 450 nm by a dimer signal at 405 nm. These spectral characteristics likely result from the close proximity of the TTF moieties on the polymer backbone (rather than diffusion controlled dimerization of TTF itself). Such findings suggest robust electronic interactions between TTF and MoS_2, with the extent of doping amplified by employing macromolecular versions of TTF. Additionally, the affinity between MoS_2 and TTF-containing polymers is supported further by the short range interaction inherent to ground state charge transfer. Kelvin probe force microscopy (KPFM) was coupled with photoluminescence (PL) spectral imaging to investigate the effect of electron doping by TTF polymer **4e** on MoS_2 work function.

KPFM is an electric force scanning probe technique that exploits a capacitive interaction between a metallized cantilever probe and the underlying material. This interaction is either attractive or repulsive, depending on the sign of the work function of the probe and sample, thus measuring the local contact or surface potential contrast (SPC) between a Pt-coated atomic force probe and the underlying substrate. In the experiments described here, mechanically exfoliated MoS_2 flakes were located on a clean glass slide and the PL spectra recorded at different locations on the flake along with surface heights and SPC measurements on these areas of interest. Electronic interactions of TTF on MoS_2 were quantified by drop-casting TTF polymer **4e** on an MoS_2 flake: the coated flake was dried, and the AFM and KPFM measurements were repeated to reveal the effect of polymer doping on the MoS_2 work function from the same flake.

Fig. 6a shows the SPC image of the (undoped) MoS_2 flake on glass. The regions of interest (labelled A, B, C, and D) indicate locations where PL spectra and SPC values were measured before and after polymer doping. The PL spectra provide an indication of flake thickness,[40] with spectrally integrated PL intensity scaling approximately linearly with flake thickness between 2 and 6 atomic layers, then vanishing for thicker samples. Thus the spectral imaging provides an approximate map of layer thickness to correlate local changes in SPC. Fig. 6b shows normalized histograms of SPC values in the labelled regions of interest before and after polymer doping. The control region (A) shows a small upshift of about 80 meV representing an approximate measure of the work function change associated with only the polymer.

For B–D, there is some variation in the SPC distribution before doping, also consistent with local variations in thickness. After doping, a reproducible upshift in SPC of about 240 mV was observed. Because the SPC or contact potential is the work function difference between the Pt coated tip (5.9 eV) and the MoS_2 (monolayer is 5.38 eV), the upshift in SPC is consistent with a decrease in the ionization potential (and work function)

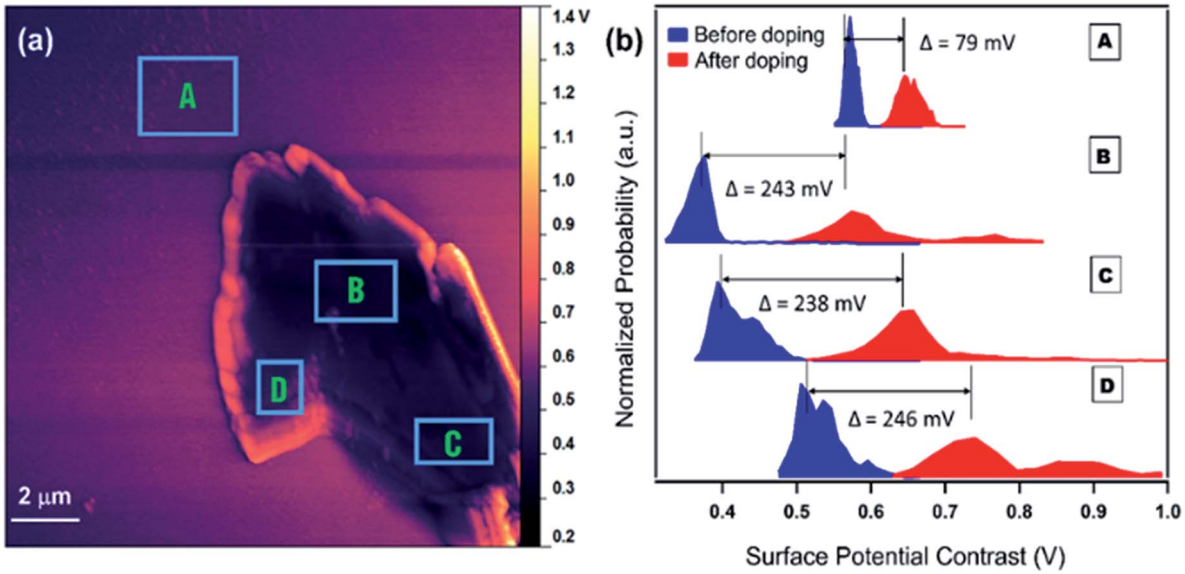

Fig. 6 Photoluminescence and Kelvin probe force microscopy on MoS_2. (a) Surface potential contrast (SPC) image of an MoS_2 flake prior to doping. (b) Normalized histograms of SPC values in selected regions of interest before (blue) and after (red) doping with **polyTTFNB-50** (**4e**) (0.001 mg mL^{-1} solution in THF). Region 'A' shows the effect of polymer only (≈5 nm layer thickness) on glass, while the doped MoS_2 shows a consistent upshift of ≈240 meV.

of MoS_2 (data on additional runs in ESI†). We additionally note a positive dependence on SPC upshift with increasing PL intensity (decreasing layer thickness) of MoS_2, consistent with a 'dilution' of the effect of carrier doping by the polymer in multi-layer MoS_2.

Conclusions

To summarize, we described novel TTF-containing polymers that afford an opportunity for non-covalent surface functionalization, band structure modulation and work-function engineering of MoS_2 nanosheets. These polymers impart solution stability of chemically exfoliated MoS_2 nanosheets, while coordinative interactions and ground state electron transfer are observed for MoS_2 with the pristine, sulfur-rich basal plane. The TTF-substituted polymers behave differently from TTF itself, readily forming TTF dimers at the polymer–MoS_2 interface that amplify surface binding and electronic interactions. TTF-based polymers afford robust, non-covalent interactions regardless of the MoS_2 lattice structure, conceptually in parallel with graphene–pyrene coordination. Tandem photoluminescence spectroscopy/Kelvin probe microscopy experiments reveal a decrease in work function for MoS_2 coated with the TTF-containing polymer. The trends elucidated experimentally are consistent with those predicted using first-principles DFT calculations, with the materials emanating from this work anticipated to accelerate MoS_2 integration into efficient devices and functional composites.

Acknowledgements

The authors acknowledge the support of the National Science Foundation (NSF-CHE-1506839) and the NSF-supported Materials Research Science and Engineering Center (MRSEC) at UMass Amherst (NSF-DMR-0820506). The authors acknowledge Dr. Alexander Ribbe at the UMass Amherst Electron Microscopy Center for assistance with high resolution transmission electron microscopy imaging.

References

1 G. Fiori, *et al.*, Electronics based on two-dimensional materials, *Nat. Nanotechnol.*, 2014, **9**(10), 768–779.
2 A. Gupta, T. Sakthivel and S. Seal, Recent development in 2D materials beyond graphene, *Prog. Mater. Sci.*, 2015, **73**, 44–126.
3 D. Sarkar, *et al.*, MoS_2 Field-Effect Transistor for Next Generation Label-Free Biosensors, *ACS Nano*, 2014, **8**, 3992–4003.
4 B. Radisavljevic, A. Radenovic, J. Brivio, V. Giacometti and A. Kis, Single-layer MoS_2 transistors, *Nat. Nanotechnol.*, 2011, **6**, 147–150.
5 S. J. Kim, *et al.*, Materials for Flexible, Stretchable Electronics: Graphene and 2D Materials, *Annu. Rev. Mater. Res.*, 2015, **45**(1), 63–84.
6 F. Bonaccorso, Z. Sun, T. Hasan and a. C. Ferrari, Graphene photonics and optoelectronics, *Nat. Photonics*, 2010, **4**, 611–622.
7 Y. Zhu, *et al.*, Graphene and graphene oxide: synthesis, properties, and applications, *Adv. Mater.*, 2010, **22**, 3906–3924.
8 R. Ganatra and Q. Zhang, Few-Layer MoS_2: A Promising Layered Semiconductor, *ACS Nano*, 2014, **8**, 4074–4099.
9 E. B. Secor, B. Y. Ahn, T. Z. Gao, J. a. Lewis and M. C. Hersam, Rapid and Versatile Photonic Annealing of Graphene Inks for Flexible Printed Electronics, *Adv. Mater.*, 2015, **27**, 6683.
10 Y. Nonoguchi, K. Hata and T. Kawai, Dispersion of synthetic MoS_2 flakes and their spontaneous adsorption on single-

walled carbon nanotubes, *ChemPlusChem*, 2015, **80**, 1158–1163.
11 V. Georgakilas, *et al.*, Functionalization of graphene: covalent and non-covalent approaches, derivatives and applications, *Chem. Rev.*, 2012, **112**, 6156–6214.
12 R. Ballesteros-Garrido, R. Rodriguez, M. Álvaro and H. Garcia, Photochemistry of covalently functionalized graphene oxide with phenothiazinyl units, *Carbon*, 2014, **74**, 113–119.
13 C. Shan, *et al.*, Water-soluble graphene covalently functionalized by biocompatible poly-L-lysine, *Langmuir*, 2009, **25**, 12030–12033.
14 D. Parviz, *et al.*, Dispersions of Non-Covalently Functionalized Graphene with Minimal Stabilizer, *ACS Nano*, 2012, **6**, 8857–8867.
15 K. C. Knirsch, *et al.*, Basal-Plane Functionalization of Chemically Exfoliated Molybdenum Disulfide by Diazonium Salts, *ACS Nano*, 2015, **9**, 6018–6030.
16 J. Huang and V. P. Dravid, Ligand Conjugation of Chemically Exfoliated MoS_2, *J. Am. Chem. Soc.*, 2013, **135**, 4584–4587.
17 K. Zhao, *et al.*, A non-covalent functionalization approach to improve the dispersibility and properties of polymer/MoS_2 composites, *Appl. Surf. Sci.*, 2014, **316**, 237–244.
18 B. Ou, *et al.*, Covalent functionalization of graphene with poly(methyl methacrylate) by atom transfer radical polymerization at room temperature, *Polym. Chem.*, 2012, **3**, 2768.
19 S. Dey, H. S. S. R. Matte, S. N. Shirodkar, U. V. Waghmare and C. N. R. Rao, Charge-transfer interaction between few-layer MoS_2 and tetrathiafulvalene, *Chem.–Asian J.*, 2013, **8**, 1780–1784.
20 X. Tian, *et al.*, Effects of 3d transition-metal doping on electronic and magnetic properties of MoS_2 nanoribbons, *Phys. Chem. Chem. Phys.*, 2015, **17**, 1831–1836.
21 X. Lin and J. Ni, Charge and magnetic states of Mn-, Fe-, and Co-doped monolayer MoS_2, *J. Appl. Phys.*, 2014, **116**, 044311.
22 S. Ana, G. Gonza and A. Jose, High Electronic Conductivity Molybdenum Disulfide-Dialkylamine Nanocomposites, *Chem. Mater.*, 1999, **11**, 2296–2298.
23 W. Osim, A. Stojanovic, J. Akbarzadeh, H. Peterlik and W. H. Binder, Surface modification of MoS_2 nanoparticles with ionic liquid-ligands: towards highly dispersed nanoparticles, *Chem. Commun.*, 2013, **49**, 9311–9313.
24 D. Kiriya, *et al.*, Air-stable surface charge transfer doping of MoS_2 by benzyl viologen, *J. Am. Chem. Soc.*, 2014, **136**, 7853–7856.
25 Y. Jing, X. Tan, Z. Zhou and P. Shen, Tuning electronic and optical properties of MoS_2 monolayer *via* molecular charge transfer, *J. Mater. Chem. A*, 2014, **2**, 16892–16897.
26 D. Canevet, M. Sallé, G. Zhang, D. Zhang and D. Zhu, Tetrathiafulvalene (TTF) derivatives: key building-blocks for switchable processes, *Chem. Commun.*, 2009, 2245–2269.
27 M. L. Kaplan, R. C. Haddon, F. Wudl and E. D. Feit, Preparation of some monophenyltetrathiafulvalenes and (*p*-vinylphenyl)tetrathiafulvalene and its polymerization, *J. Org. Chem.*, 1978, **43**, 4642–4646.
28 Y. F. Liang, C. U. Pittman and M. Ueda, Synthesis and Polymerization of *p*-(2-Tetrathiafulvalenyl)phenyl Methacrylate, *J. Org. Chem.*, 1979, **44**, 3639–3642.
29 T. Shimizu and T. Yamamoto, Preparation of a new poly(arylacetylene) with a tetrathiafulvalene (TTF) unit in the side chain, *Chem. Commun.*, 1999, 515–516, DOI: 10.1039/a900300b.
30 J. A. Love, J. P. Morgan, T. M. Trnka and R. H. Grubbs, A practical and highly active ruthenium-based catalyst that effects the cross metathesis of acrylonitrile, *Angew. Chem., Int. Ed.*, 2002, **41**, 4035–4037.
31 Y.-S. Shon and T. Randall Lee, Catalytic ring-closing olefin metathesis of sulfur-containing species: heteroatom and other effects, *Tetrahedron Lett.*, 1997, **38**, 1283–1286.
32 C. W. Bielawski and R. H. Grubbs, Increasing the Initiation Efficiency of Ruthenium-Based Ring-Opening Metathesis Initiators: Effect of Excess Phosphine, *Macromolecules*, 2001, **34**, 8838–8840.
33 P. T. Chiang, N.-C. Chen, C. C. Lai and S.-H. Chiu, Direct observation of mixed-valence and radical cation dimer states of tetrathiafulvalene in solution at room temperature: association and dissociation of molecular clip dimers under oxidative control, *Chem.–Eur. J.*, 2008, **14**, 6546–6552.
34 L. Huchet, *et al.*, Spectroelectrochemistry of Electrogenerated Tetrathiafulvalene-Derivatized Poly(thiophene): Toward a Rational Design of Organic Conductors with Mixed Conduction, *J. Phys. Chem. B*, 1998, 5647.
35 P. Joensen, R. F. Frindt and S. R. Morrison, Single-layer MoS_2, *Mater. Res. Bull.*, 1986, **21**, 457–461.
36 A. Splendiani, *et al.*, Emerging photoluminescence in monolayer MoS_2, *Nano Lett.*, 2010, **10**, 1271–1275.
37 T. J. Wieting and J. L. Verble, Infrared and Raman Studies of Long-Wavelength Optical Phonons in Hexagonal MoS_2, *Phys. Rev. B: Solid State*, 1971, **3**, 4286–4292.
38 M. Yoshizawa, K. Kumazawa and M. Fujita, Room-temperature and solution-state observation of the mixed-valence cation radical dimer of tetrathiafulvalene, $[(TTF)_2]^+$, within a self-assembled cage, *J. Am. Chem. Soc.*, 2005, **127**, 13456–13457.
39 J. M. Spruell, *et al.*, Highly stable tetrathiafulvalene radical dimers in [3]catenanes, *Nat. Chem.*, 2010, **2**, 870–879.
40 Eda, *et al.*, Photoluminescence from Chemically Exfoliated MoS_2, *Nano Lett.*, 2011, **11**, 5111–5116.